2023-1

Low-fidelity design optimization and parameter sensitivity analysis of tilt-rotor eVTOL electric propulsion systems

Tyler Critchfield
Brigham Young University - Provo, trcritchfield@gmail.com

Andrew Ning
Brigham Young University - Provo, aning@byu.edu

Original Publication Citation

Critchfield, T. and Ning, A., "Low-fidelity design optimization and parameter sensitivity analysis of tilt- rotor eVTOL electric propulsion systems," AIAA SCITECH Forum, National Harbor, MD, Jan 2023. doi: 10.2514/6.2023-0325

Low-fidelity design optimization and parameter sensitivity analysis of tilt-rotor eVTOL electric propulsion systems

Tyler Critchfield* and Andrew Ning†
Brigham Young University, Provo, Utah, 84602

Urban air mobility requires a multidisciplinary approach to tackle the important challenges facing the design of these aircraft. This work uses low-to-mid fidelity tools to model rotor aerodynamics, blade structures, vehicle aerodynamics, and electric propulsion for a tilt-rotor electric vertical takeoff and landing (eVTOL) aircraft. We use gradient-based design optimization and extensive parameter sensitivity analysis to explore the design space and complex tradeoffs of tilt-rotor distributed electric propulsion systems.

Nomenclature

AR	=	wing aspect ratio
b	=	wing span
c	=	chord
C	=	battery capacity
c_σ	=	bending moment arm
C_{D_P}	=	parasitic drag coefficient
D	=	drag
e	=	Oswald efficiency factor
e_{inv}	=	inviscid span efficiency
I_σ	=	moment of inertia
L	=	lift
m	=	mass
M	=	blade bending moment
n_p	=	# battery cells in parallel
n_s	=	# battery cells in series
OCV	=	battery open current voltage
q	=	dynamic pressure
Q	=	torque
r	=	radial location along the blade
R_b	=	battery internal resistance
R_m	=	motor resistance
R_{tip}	=	blade radius
S	=	wing area
SOC	=	battery state of charge
t	=	time
v_b	=	battery output voltage
v_e	=	motor back emf
v_m	=	motor voltage
V_∞	=	freestream velocity
Ω	=	rotational speed in rad/sec
ρ	=	density
σ	=	bending stress

*Doctoral Candidate, Mechanical Engineering, AIAA Student Member
†Associate Professor, Mechanical Engineering, AIAA Associate Fellow

I. Introduction

Urban air mobility (UAM) is an emerging technological development that has the potential to revolutionize modern transportation systems. It presents a challenging problem that requires careful study from multiple disciplines to approach aircraft designs that are feasible, quiet, and economically viable. Electric vertical takeoff and landing (eVTOL) aircraft are a subset of UAM that present intriguing challenges and payoffs. Notably, these aircraft could operate effectively in dense, urban areas with low environmental emissions and without the need for a traditional runway. NASA researchers have introduced several conceptual design configurations for these eVTOL aircraft, including single- and multi-rotor helicopters and designs that obtain cruise lift from wing lifting surfaces such as the tilt-rotor, tilt-wing, and lift+cruise concepts [1–5].

These various configurations come with interesting design tradeoffs. Of particular interest in this study is the tilt-rotor configuration, where rotors provide vertical lift to the aircraft and then these same rotors rotate to provide thrust in forward flight while the wing provides lift like a typical aircraft. Lift provided by the wing instead of rotors during cruise is much more energy efficient, which this design shares with the lift+cruise concept. A benefit to using the same rotors for vertical and forward flight is a weight reduction of not needing to haul lift rotors during cruise that only create more drag. A downside to this configuration is that a rotor needing to operate in both hover and cruise will not be the best performing rotor for either stage of flight.

When approaching the design of eVTOL propulsion systems, including rotor and blade design, it is helpful to use a mission-based perspective or else important considerations can be overlooked. This is especially true for tilt-rotor designs. Rotors that are engineered to perform well in both hover and cruise need high-level mission analysis or else the final design will become an arbitrarily weighted average of the optimal designs of the two cases, without great reason for whether it should be more weighted toward the cruise or hover scenarios. A mission-based objective helps solve this problem (for instance, by optimizing range or endurance rather than aerodynamic efficiency in one of the stages).

Multidisciplinary design optimization is an important tool to understand these complex and relatively new design spaces under a mission-focused framework. Several studies have used design optimization to model UAM conceptual aircraft and high-level mission parameters, including Stoll et. al [6], Brown and Harris [7], Ha et. al [8], Lee et. al [9], and Saetti et. al [10]. Design optimization has also been used in studies more focused on rotor blade design [11–13]. To better understand the complex tradeoffs between performance in hover and cruise for the same rotors, we must combine rotor and blade design optimization with a mission-focused objective.

Some studies have combined these efforts to model aircraft geometry along with mission-level performance. Hwang and Ning [14] and Moore and Ning [15] had such an approach to the NASA X-57 short-takeoff and landing aircraft concept. Clarke et. al approached this problem with a specific focus on blown-wing analysis [16]. Hendricks et. al did this for a quadrotor eVTOL configuration [17], as well as a turbo-electric tilt-wing concept [18] where they modeled propeller performance with blade element momentum theory along with a wing aerostructural model, electric system, and flight dynamics.

This work approaches a similar problem by applying high-level multidisciplinary design optimization to a fully-electric tilt-rotor eVTOL aircraft configuration. Our focus is to study propeller blade geometries and mission-level performance tradeoffs for tilt-rotor propulsion systems that must operate effectively in vertical flight and cruise conditions. We model propeller aerodynamics using blade element momentum theory and blade structures, vehicle aerodynamics, and electric propulsion using low-fidelity methods. We place a special emphasis on parameter sensitivity analysis of such optimizations, seeking to understand how specific parameter variations affect mission-level performance and optimal blade geometries.

II. Methods

The following sections describe the mission profile, optimization approach, and models used in this work, including models for propeller aerodynamics, electric propulsion, vehicle drag, and blade structures.

A. Mission

We optimize electric propulsion systems for a generic tilt-rotor vehicle configuration with parameters listed in Table 1. The propulsion system is modeled under vertical flight and cruise conditions (see Fig. 1). We focus on mission-level performance and neglect controller optimization in our work, so transition flight is neglected. Time in the vertical flight stages is fixed while time in cruise is determined based on available energy and power requirements. We also include a reserve mission the system is required to complete that consists of traveling an additional six miles at a lower altitude, per standards from Uber Elevate [19].

Table 1 Parameters used for the tilt-rotor configuration in this study.

Parameter	Value
# rotors	6
# blades per rotor	5
non-battery weight	2600 lbs
wing span	11 m
wing area	12 m^2

Rotor and blade geometries remain fixed for the entire mission while we allow rotational speed to vary between the stages. We also include a collective pitch in cruise to adapt for higher cruising velocities. In addition, we analyze each design using a one-engine-out scenario so the system is able to handle the necessary thrust and power requirements when one of the rotors is non-functioning. (Though in this scenario we are neglecting asymmetric loading caused by such an event.)

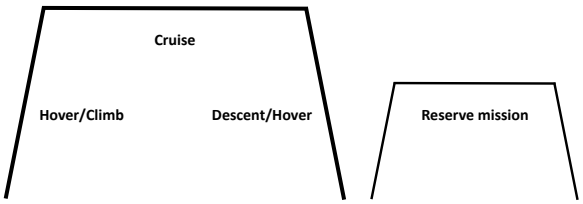

Fig. 1 Mission profile used in this work - the reserve mission consists of traveling six additional miles in cruise conditions.

B. Propeller aerodynamics

The propeller aerodynamics are modeled using blade element momentum (BEM) theory. BEM has been used extensively in propeller analysis [11, 12, 14–18]. BEM combines a momentum balance and airfoil analysis along the radius of the rotor blade. Using the method described in [20, 21], a solution can be found from combining these two analyses that is continuous and guaranteed to converge, making it ideal for design optimization. We use the implementation in CCBlade.jl*, which is able to calculate exact derivatives using forward-mode algorithmic differentiation. CCBlade is able to compute derivatives efficiently without needing to pass them through every iteration of its internal solver†.

For the studies in this work, we use the MH117 airfoil with precomputed rotational corrections (Du Selig for lift [22] and Eggers for drag [23]) based on blade properties at 75% of the blade radius and extrapolated to high angles of attack using the Viterna method [24]. We employ hub and tip loss corrections from Prandtl [25] that account for the induced velocities from the hub and tip vorticies. We also include a correction for the induction factor from Buhl [26] that is a modification of Glauert's method [27]. We assume steady inflow conditions and no interactions between blade sections. We additionally neglect aerodynamic interactions between adjacent rotor wakes and between wakes and vehicle surfaces.

C. Propulsion System

The electric propulsion model combines the propeller model from the previous section with a basic motor and battery model. The equivalent circuit model for the DC electric motor is shown in Fig. 2 where v_m is the motor voltage supplied from the battery (via the motor controller), v_e is the back emf, and R_m is the motor internal resistance. This model computes the steady-state behavior of the motor, which is appropriate in this application where the time constant associated with propulsive power changes is much larger than any time constant of the circuit. If transient responses

*https://github.com/byuflowlab/CCBlade.jl
†https://github.com/byuflowlab/ImplicitAD.jl

were important, for example in a more detailed exploration of the power fluctuations during transition, then this motor model should include an inductor. All the motors are assumed to be identical and in parallel, with their own speed controllers, each powered by a separate yet identical battery.

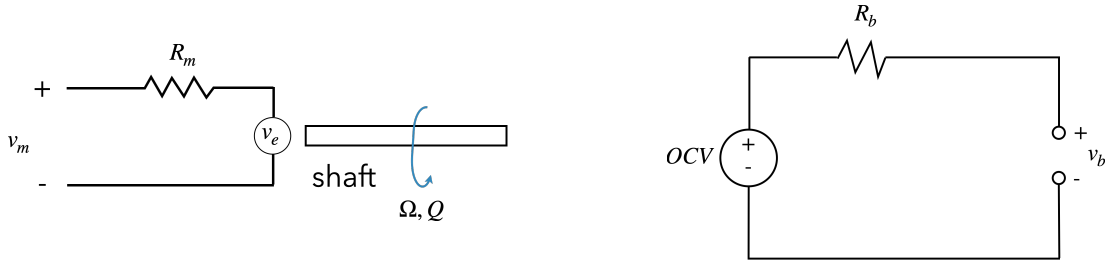

Fig. 2 Equivalent circuit models for a basic motor (left) and battery (right).

The equivalent circuit model of the battery is shown in Fig. 2 where OCV is the open circuit voltage, R_b is the internal resistance of the battery, and v_b is the output voltage from the battery. Again, the time constants associated with power changes are large compared to the circuit time constants, but if not one should add a capacitor branch to the circuit.

In this paper we use the Panasonic NCR18650G cell, which has a capacity of 3.55 Amp-h and a mass of 48 grams (resulting in a specific energy of about 135 Wh/kg). Higher specific energies could be obtained with a customized battery, but this provides a reasonable representation of current technology, especially as we assume that all values represent an end-of-life state so that no additional degradation model is used. This battery has also been used in previous studies for eVTOL applications making for a helpful comparison [28]. Both the internal resistance and the open current voltage are functions of the batteries state of charge, and for this battery a data fit was provided by [29] (although we refit the OCV as a quadratic rather than sixth-order polynomial for simplicity).

$$OCV(SOC) = 0.39\ SOC^2 + 0.07\ SOC + 3.7 \tag{1}$$

$$R(SOC) = 0.015\ SOC^2 - 0.025\ SOC + 0.104 \tag{2}$$

The battery pack is made of a number of cells arranged in various modules and submodules. For our purposes, the details of the arrangement are not essential, but we do need to know the total number of cells in series (n_s) and the total number of cells in parallel (n_p). We include a 20% markup on the battery mass to account for wiring, the battery management system, and other overhead required in the pack beyond just the cells. We also ensure that the battery power margin is positive (i.e., the total requested power does not exceed the maximum power available from the battery).

After each mission segment that occurs over some time interval t, we update the state of charge based on battery current and capacitance. To avoid premature battery degradation at both top and bottom of charge we don't allow SOC to exceed 0.9 or drop below 0.2. Our assumed mission uses all of this state of charge, though we recognize that other missions may not want to deplete the battery each flight for quicker turnaround times. For the cruise portion of the mission we use this overall battery usage assumption to analytically solve for the cruise endurance based on the given power requirements in each phase of the mission.

D. Aircraft Aerodynamics

We implement the following simplified drag model to estimate induced and parasitic drag based on vehicle size and weight. We also include a 10% drag markup to account for wake mixing and other effects not captured by this low-fidelity analysis.

$$D = C_{D_P} q S + \frac{L^2}{q \pi b^2 e} \tag{3}$$

C_{D_P} is the parasitic drag coefficient, q is the dynamic pressure, S is the wing area, b is the wing span, and e is the Oswald efficiency factor (see Eq. (4)). Our estimated values for C_{D_P} and e_{inv} are 0.033 and 0.94, respectively. Our optimal designs resulted in an effective lift-to-drag ratio of approximately 11.

$$e = \frac{1}{\frac{1}{e_{inv}} + 0.38\pi C_{D_P} AR} \tag{4}$$

E. Blade structures

We implemented a simple bi-axial bending stress model to the rotor blade to ensure the designs were structurally sound. We modeled the blade as a cantilever beam and calculated bending moments from the BEM axial and tangential loading at each blade section. From there we determined bending stress (see Eq. (5)) using a simplified spar cap model to determine the moment of inertia. We assumed a spar cap thickness of 10% of the cross section thickness and a width equal to half the chord length.

$$\sigma = \frac{M_x c_{\sigma_x}}{I_{\sigma_x}} + \frac{M_y c_{\sigma_y}}{I_{\sigma_y}} \tag{5}$$

Here c_σ is the distance from the center of the cross section to the point of interest, which in this case was at the corners of the spar cap. We then constrained the total axial stress to be less than the compressive and tensile strengths of high modulus carbon fiber reinforced polymer (CFRP) tape: 800 MPa and 700 MPa, respectively. We also applied an additional safety factor of 1.5 to the bending stress.

F. Optimization Approach

Optimizations in this work use Sparse Nonlinear OPTimizer (SNOPT) [30], an SQP algorithm for gradient-based constrained optimization. Providing the optimizer with exact derivatives is ideal to preserve accuracy and save computational cost. Derivatives in our framework are evaluated using forward-mode algorithmic differentiation (AD) [31].

For the optimization studies in this work we maximized range with design variables that include rotor radius, blade chord and twist distributions, collective pitch, freestream velocity, rotational speed for both hover and cruise states, and the number of battery cells in series and in parallel. We constrain the design with minimum thrust, maximum bending stress, maximum Mach tip speed, and maximum battery power output restrictions. These optimization parameters are summarized in Eq. (6).

$$\begin{aligned}
&\textit{maximize} && \text{range} \\
&\textit{with respect to} && R_{tip} \\
&&& \text{chord (7)} \\
&&& \text{twist (7)} \\
&&& \text{collective pitch} \\
&&& V_\infty \\
&&& \Omega_{cruise} \\
&&& \Omega_{hover} \\
&&& \#\text{ battery cells in series, } ns \\
&&& \#\text{ battery cells in parallel, } np \\
&\textit{subject to} && \text{minimum thrust} \\
&&& \quad \text{hover: thrust} \geq \text{total weight} \\
&&& \quad \text{cruise: thrust} \geq \text{total drag} \\
&&& \text{maximum biaxial bending stress} \\
&&& \text{maximum Mach tip speed} \leq 0.6 \\
&&& \text{battery power margin} \geq 0
\end{aligned} \tag{6}$$

Chord and twist distributions were modeled with Akima splines. The number of battery cells in series and parallel are integer quantities, but for compatibility with gradient-based optimization we include them as continuous design variables in the battery equations. After optimization we round to the nearest integer, then re-optimize all remaining design variables (dynamic rounding). While battery pack design requires additional considerations, which would likely require adjusting the total number of cells, this level of modeling at least captures the tradeoffs in battery mass with voltage and current requirements.

The design is required to have enough thrust in cruise to match the estimated drag of the vehicle. In hover/climb/descent phases this thrust requirement is the gross weight of the aircraft, which includes the fixed structural/payload weight and the total battery weight. Both thrust requirements include a 20% markup for safety precautions. As previously described, the bending stress constraint includes a safety factor of 1.5. The blade tip speed is restricted to Mach 0.6 or lower to restrict the noise output and avoid transonic fluid behavior. Finally, the power margin of the batteries in each phase needs to be positive to ensure the batteries are capable of providing the maximum power required by the motors during flight.

III. Results and Discussion

Using the methods described in the previous section, we performed gradient-based design optimization on tilt-rotor electric propulsion systems with the optimization parameters outlined in the previous section. Fig. 3 shows the chord planform and twist distribution for an example optimization and Table 2 lists other parameter values for the optimized design. This design resulted in a range (outside of reserves) of 136.4 km and a cruise endurance of 37.2 minutes.

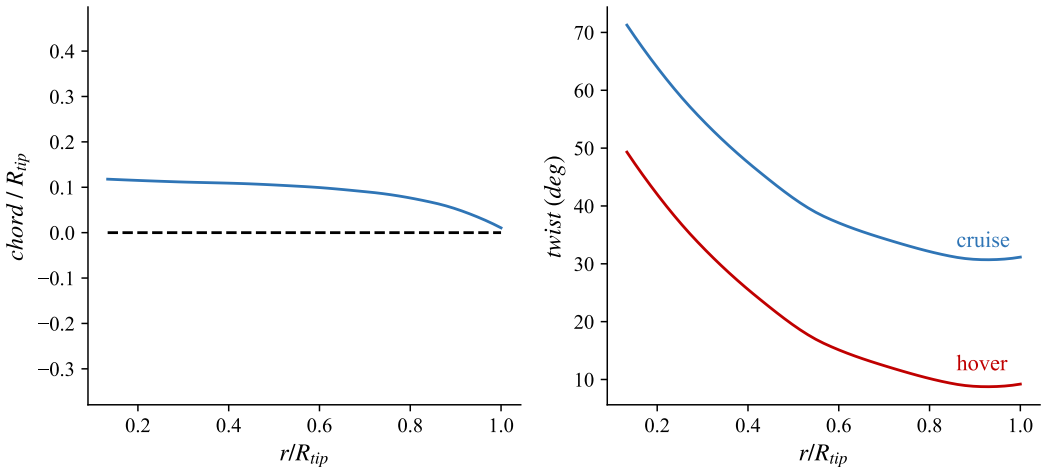

Fig. 3 Example optimized rotor blade planform and twist profiles.

Fig. 4 shows the progression of state of charge through the course of the mission, including the reserve segment, as well as the proportional usage of the battery among the three main mission stages (vertical flight, cruise, and reserve). For this optimal design, the cruise stage uses about half of the available battery energy. Vertical flight uses a little more than a third and reserves use about one-sixth of the available battery energy. We should note that we are being extra-conservative with our power estimates here as we've lumped climb and hover together as vertical flight.

With low-fidelity models, the optimal design matters less than the ability to understand the design space and explore unique tradeoffs and sensitivities of the design to specific parameters. We analyzed such sensitivities for the following parameters: non-battery weight, time in hover/vertical flight, battery specific energy, rotor blade count, and blade radius. Fig. 5 shows sensitivities of the range to each of the parameters. Vehicle non-battery weight, time spent in hover/vertical flight phases, and battery specific energy have large significant effects on total range that appear to show linear relationships. Increasing blade count has a slight negative effect on range while blade radius appears to have little to no effect on the range unless it is restricted to low values where optimizations struggle to converge with feasible designs.

Table 2 Optimized design parameters.

Parameter	Optimized Value
R_{tip}	1.73 m
collective pitch	21.99 deg
V_∞	136.9 mph
Ω_{cruise}	674.1 RPM
Ω_{hover}	1126.2 RPM
ns	59
np	99
battery weight fraction	58.9%

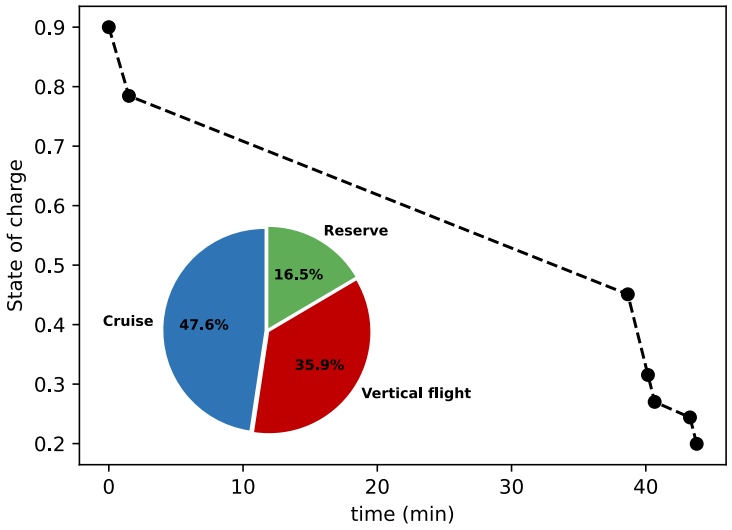

Fig. 4 Battery state of charge over the course of the entire mission and the amount of battery usage in each of the three major phases of the mission: vertical flight, cruise, and reserve (embedded).

A. Sensitivity to structural and payload weight

Fig. 6 shows the blade design and range sensitivities to changing the structural and payload weight of the aircraft. This weight has a significant effect on range, where a decrease in weight of 100 lbs can lead to an increase in range of about 30 km (see part (b)). This non-battery weight has a slight effect on the blade geometry, where chord increases while twist decreases slightly with increasing weight (see part (a)). Notably, however, the optimizer primarily chooses to increase blade radius to provide more thrust instead of increasing chord substantially.

Part (c) of this figure shows that Ω decreases substantially in both hover and cruise phases, presumably to allow the radius to increase while preserving the Mach tip speed constraint. In fact, for every sensitivity presented in this study, Ω_{hover} has a consistent, inverse relationship with radius as the Mach tip speed constraint is always active in vertical flight. This makes sense as that is the portion of the mission that requires the most thrust and power. Here, the optimizer appears to find more benefit in increasing radius and decreasing Ω rather than the inverse to supply an increase in thrust. This also makes sense as increased rotational speed will, in general, have more of a negative impact on power required by the motors and thus will expend energy more quickly.

Another interesting observation to note is that the optimal cruise velocity and battery size remain relatively unchanged with increasing non-battery weight. (Battery size, for instance, is only decreased by about 5% despite an increase in non-battery weight of 50%.) This seems to suggest that there is only so much battery weight that can support itself.

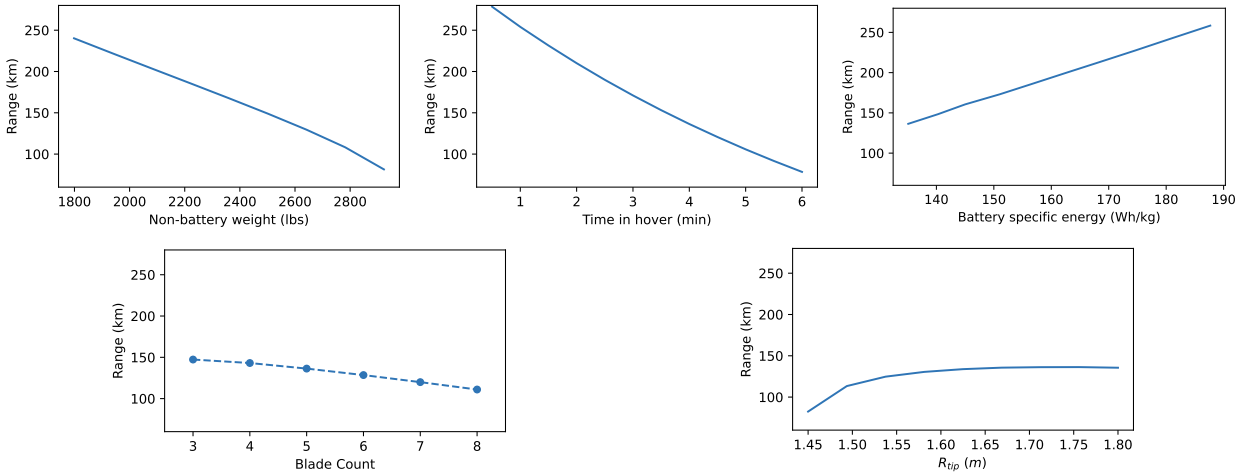

Fig. 5 Design sensitivities of range to system parameters.

The aircraft cannot simply add more batteries to account for the increase in thrust requirement added by the increased weight. Increasing battery weight does increase available energy, but it does so at the cost of increased thrust and power required, which then requires more energy. This sensitivity study highlights this difficult tradeoff and reminds us of the ever-present reduction in aircraft performance with increasing weight.

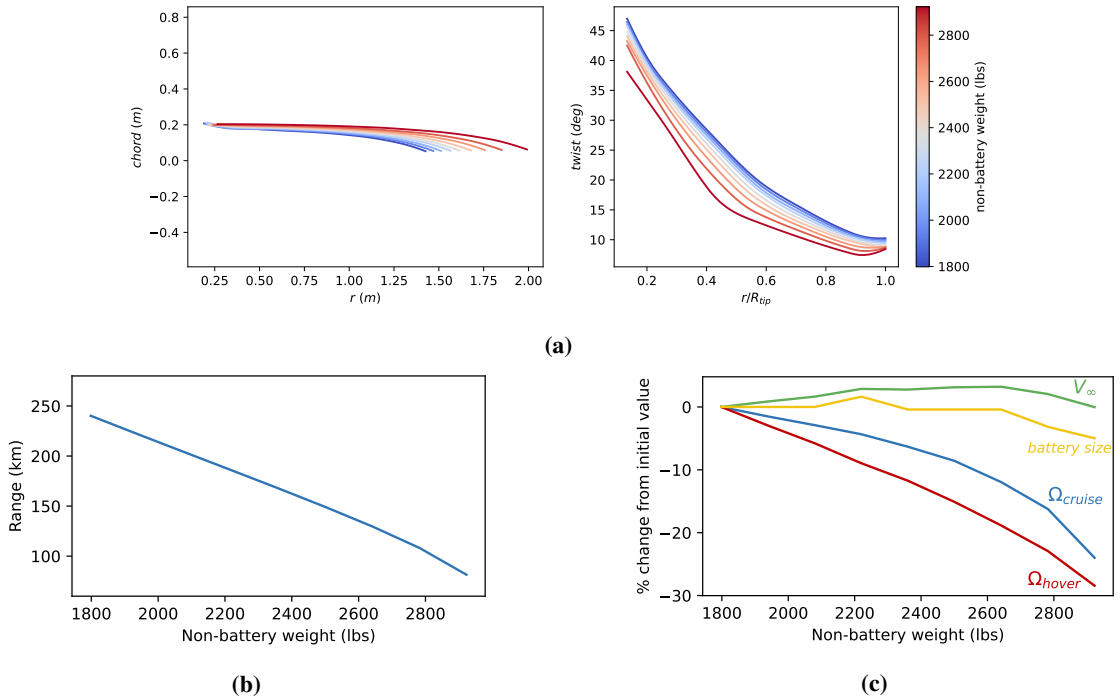

Fig. 6 Design sensitivity to non-battery weight ranging from 1800 to 2900 lbs. Each curve represents a different weight which was fixed while the design was re-optimized.

B. Sensitivity to time in hover/vertical flight

Fig. 7 shows the design sensitivities to time spent in hover/vertical flight. These results are comparable to the weight sensitivities as the range is significantly affected by increased time in this flight stage while the blade geometry is only

affected slightly. Again, the optimizer slightly decreases twist throughout the blade and increases blade radius as time in hover increases, though chord remains unchanged. This makes intuitive sense as the hover flight stage requires more thrust and thus will deplete the battery more quickly, leaving less time to travel in the cruise stage.

According to this relationship, every additional minute in vertical flight reduces available cruise endurance by approximately ten minutes (see part (b)). From this high-level study, at least, we are reminded that time in vertical flight should be kept to a minimum. (We are, of course, neglecting other factors that may incentivize more vertical flight time, such as flying at a higher altitude to reduce noise emissions.)

We can learn from part (c) that battery size is more significantly affected by time in vertical flight than it was for structural/payload weight. Increasing time in hover/vertical flight by 5 minutes reduces the battery size by about 10%. So not only does the aircraft use more energy in hover and thus leaves less available energy for use in forward flight, but using that extra energy incentivizes the design to decrease the total battery energy to maximize range. Thus the tradeoff of adding more battery weight to meet increased energy demand becomes even stricter.

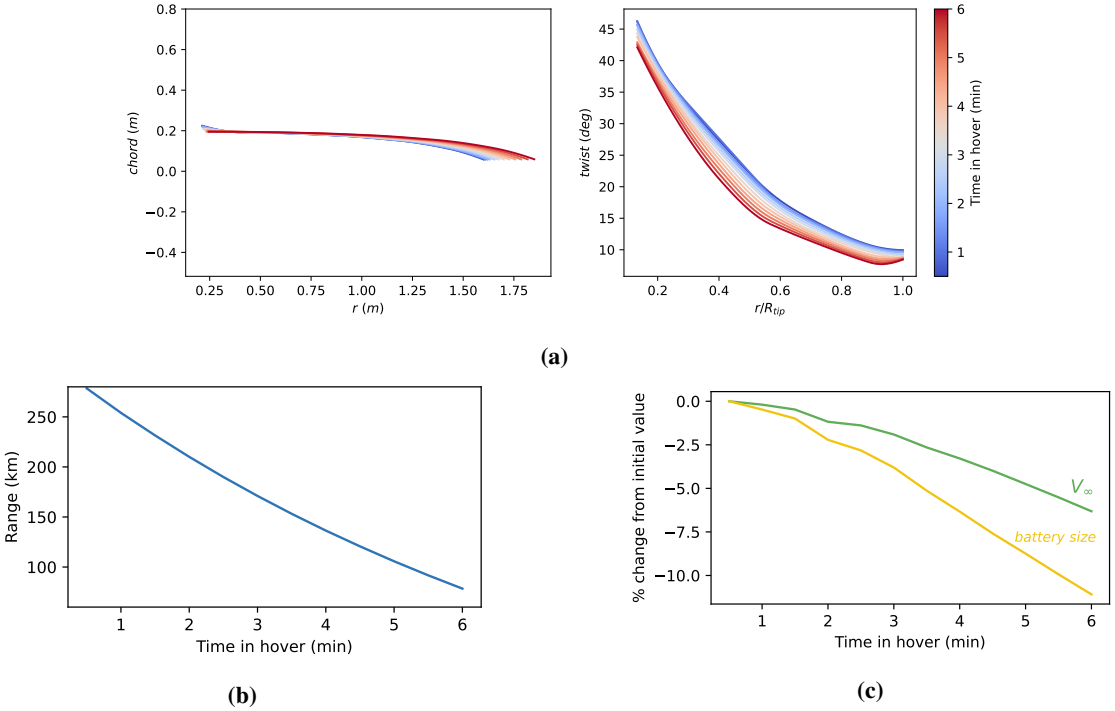

Fig. 7 Design sensitivity to total time spent in hover/vertical flight ranging from 30 sec to 6 min.

C. Sensitivity to battery specific energy

Fig. 8 shows sensitivities with respect to battery specific energy. Higher energy density of the batteries means the system can have the same available energy for a lower weight penalty. As expected, range has a large positive relationship with battery specific energy; as energy density increases, range increases by a significant amount (see part (b)). For example, a 5% increase in battery specific energy leads to an increase of 12% in optimal range. However, the optimal designs here are not simply recycled from before with more energy to fly farther in cruise; the previously discussed tradeoff between additional battery energy and weight is changing. As can be seen in part (c) of the figure, the optimal propulsion system adds more battery as its energy density increases. Thus the penalty for adding additional battery weight is less severe, or rather delayed until a higher battery weight fraction is achieved.

We observe some interesting behavior of the blade geometry profiles due to this adjustment in battery weight (see part (a)). As specific energy increases, the blade radius actually decreases (with a corresponding increase in rotational speed). This is not typical behavior compared to the other sensitivity studies, considering the extra battery weight will require more thrust, not less. To provide necessary thrust and account for the increased bending stresses supplied by the higher rotational speed of the rotor, the optimizer increases twist throughout the blade and increases chord near the

root. Thus, optimal tilt-rotor designs engineered based on current battery capabilities will look different than ones that prepare for future battery capabilities. Optimal range, according to this high-level analysis for tilt-rotor eVTOL systems, will not be maintained if blade designs remain fixed and fly with more energy rather than adjusting as battery energy density improves in the future.

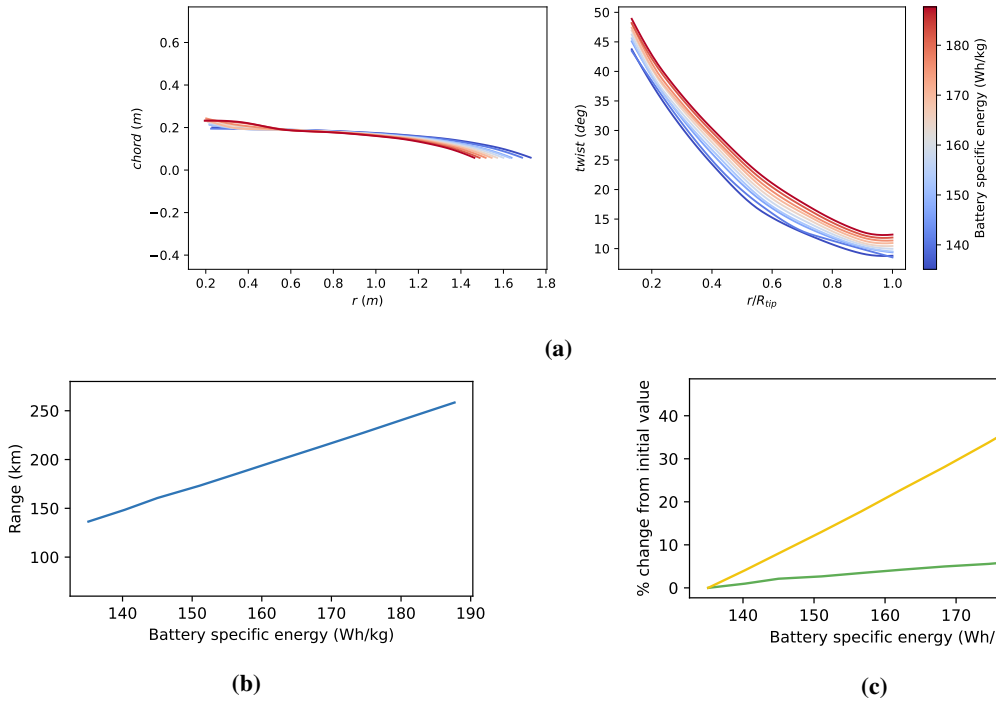

Fig. 8 Design sensitivity to the battery cell capacity ranging from 135 to 188 Wh/kg.

D. Sensitivity to blade count

Blade count has a slight effect on range, as shown in Fig. 9, though not nearly as much of an effect as other parameters in this study. This time the chord and twist distributions are affected more: as blade count decreases, the chord planform increases along with radius to supply the same amount of thrust while twist also increases slightly. The optimizer appears to be aiming for a similar rotor solidity.

Interestingly, while battery size and freestream velocity remain relatively unchanged (and thus are not shown here), rotational speed in hover and in cruise do not behave similarly as they have with other parameter variations (see part (c)). Typically Ω_{hover} exhibits an inverse relationship to blade radius, as we previously discussed. This holds true here as well. However, Ω_{cruise} has the opposite relation in this case. The parameters we have studied so far have had a similar though less pronounced effect on Ω_{cruise} as they have on Ω_{hover}. In this case, when blade count is lowered, the optimizer raises radius while also raising rotational speed in cruise as the Mach tip speed constraint is not yet active in forward flight.

While it appears from this simple analysis that fewer blades is optimal for a tilt-rotor design, the effect is small enough that more comprehensive analysis is needed to understand this effect. For instance, in our work we have largely neglected acoustic effects and higher-fidelity structural models that would be instructive to better understand these tradeoffs.

E. Sensitivity to blade radius

Finally, we study the effect of changing the blade radius. In these optimization runs the radius is a fixed constant and no longer a design variable. This could pertain to situations where the rotor radius is limited by proximity to other rotors or for manufacturing feasibility. Except for radii lower than 1.5 m, range appears to be largely unaffected by the radius. Chord and twist are largely unaffected, except for twist near the tip of the blade which steadily decreases with

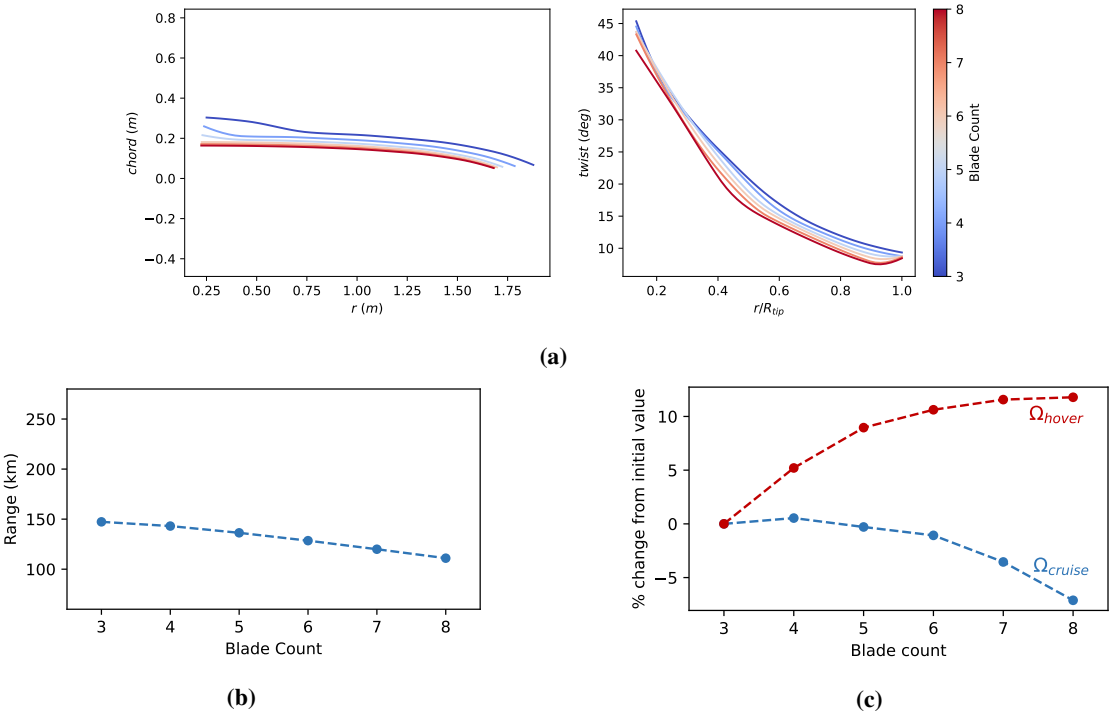

Fig. 9 Design sensitivity to rotor blade count.

increasing blade radius. As the radius approaches the minimum of this range (any lower was difficult to find feasible designs whose optimizations converged properly), there is a sudden change in the geometry profiles, where the root chord increases and the root twist decreases. At this and lower radii, the system struggles to maintain enough thrust while still allowing for enough energy to complete the mission and reserves.

The optimizer does not always seek to maximize radius in these cases. Generally increasing the radius while decreasing Ω has allowed for the most efficient energy savings while increasing thrust, but this only holds to a certain point. At very high radii, it becomes more and more difficult to maintain feasibility (including satisfying thrust, Mach tip speed, power margin, and bending stress constraints) without sacrificing more energy than it is worth.

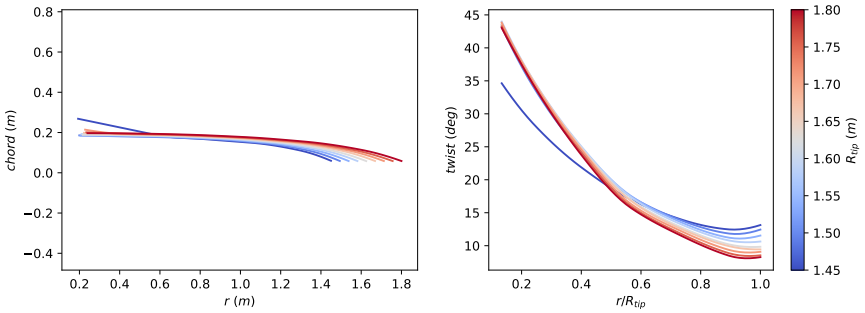

(a)

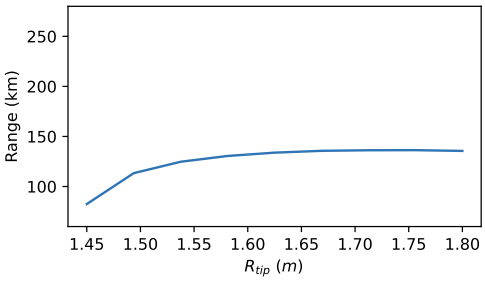

(b)

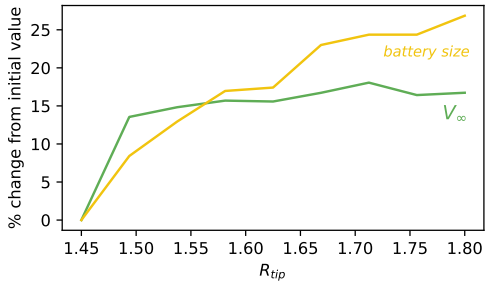

(c)

Fig. 10 Design sensitivity to rotor blade radius ranging from 1.45 to 1.8 m.

IV. Conclusion

We analyzed a tilt-rotor electric propulsion system, including blade geometries, using gradient-based design optimization with blade element momentum (BEM) theory for propeller performance and low-fidelity models for vehicle aerodynamics, blade structures, and motor and battery performance. We extensively studied parameter design sensitivities and have highlighted parameters that have a significant effect on available range for a conceptual tilt-rotor eVTOL aircraft. Future work needs to be done to understand these design tradeoffs more deeply by introducing more comprehensive models among the various disciplines. We expect to build upon this work by introducing a geometrically exact beam model for better structural analysis of the rotor blades as well as tonal and broadband acoustic models to capture the effect of propulsion system design on noise emissions during the various stages of a tilt-rotor mission.

V. Acknowledgements

The material presented in this paper is based upon work supported by NASA under award No. 80NSSC21M0070.

References

[1] Johnson, W., and Silva, C., "Observations from exploration of vtol urban air mobility designs," *7th Asian/Australian Rotorcraft Forum*, 2018.

[2] Johnson, W., and Silva, C., "NASA concept vehicles and the engineering of advanced air mobility aircraft," *The Aeronautical Journal*, Vol. 126, No. 1295, 2022, pp. 59–91.

[3] Kadhiresan, A. R., and Duffy, M. J., "Conceptual Design and Mission Analysis for eVTOL Urban Air Mobility Flight Vehicle Configurations," *AIAA Aviation 2019 Forum*, 2019, p. 2873.

[4] Whiteside, S. K., Pollard, B. P., Antcliff, K. R., Zawodny, N. S., Fei, X., Silva, C., and Medina, G. L., "Design of a Tiltwing Concept Vehicle for Urban Air Mobility," Tech. rep., 2021.

[5] Moore, M., "NASA puffin electric tailsitter VTOL concept," *10th AIAA Aviation Technology, Integration, and Operations (ATIO) Conference*, 2010, p. 9345.

[6] Stoll, A. M., and Veble Mikic, G., "Design studies of thin-haul commuter aircraft with distributed electric propulsion," *16th AIAA Aviation Technology, Integration, and Operations Conference*, 2016, p. 3765.

[7] Brown, A., and Harris, W., "A Vehicle Design and Optimization Model for On-Demand Aviation," *2018 AIAA/ASCE/AHS/ASC Structures, Structural Dynamics, and Materials Conference*, 2018.

[8] Ha, T. H., Lee, K., and Hwang, J. T., "Large-scale design-economics optimization of eVTOL concepts for urban air mobility," *AIAA Scitech 2019 Forum*, 2019, p. 1218.

[9] Lee, B.-S., Tullu, A., and Hwang, H.-Y., "Optimal design and design parameter sensitivity analyses of an eVTOL PAV in the conceptual design phase," *Applied Sciences*, Vol. 10, No. 15, 2020, p. 5112.

[10] Saetti, U., Enciu, J., and Horn, J. F., "Performance and design optimization of the f-helix evtol concept," *Proceedings of the Vertical Flight Society's 75th Annual Forum and Technology Display, Philadelphia, PA, USA*, 2019, pp. 13–16.

[11] Ingraham, D., Gray, J. S., and Lopes, L. V., "Gradient-Based Propeller Optimization with Acoustic Constraints," *AIAA Scitech 2019 Forum*, 2019, p. 1219.

[12] Hoyos, J. D., Jímenez, J. H., and Alvarado, P., "Improvement of Electric Aircraft Endurance through Propeller Optimization via BEM-CFD Methodology," *Journal of Physics: Conference Series*, Vol. 1733, IOP Publishing, 2021, p. 012011.

[13] Alba, C., Elham, A., German, B., and Veldhuis, L. L., "A surrogate-based multi-disciplinary design optimization framework exploiting wing-propeller interaction," *18th AIAA/ISSMO Multidisciplinary Analysis and Optimization Conference*, 2017, p. 4329.

[14] Hwang, J., and Ning, A., "Large-scale multidisciplinary optimization of an electric aircraft for on-demand mobility," *2018 AIAA/ASCE/AHS/ASC Structures, Structural Dynamics, and Materials Conference*, 2018, p. 1384.

[15] Moore, K., and Ning, A., "Takeoff and Performance Tradeoffs of Retrofit Distributed Electric Propulsion for Urban Transport," *Journal of Aircraft*, 2019. doi:10.2514/1.C035321.

[16] Clarke, M. A., Erhard, R. M., Smart, J. T., and Alonso, J., "Aerodynamic Optimization of Wing-Mounted Propeller Configurations for Distributed Electric Propulsion Architectures," *AIAA AVIATION 2021 FORUM*, 2021, p. 2471.

[17] Hendricks, E. S., Aretskin-Hariton, E., Ingraham, D., Gray, J. S., Schnulo, S. L., Chin, J., Falck, R., and Hall, D., "Multidisciplinary Optimization of an Electric Quadrotor Urban Air Mobility Aircraft," *AIAA AVIATION 2020 FORUM*, 2020, p. 3176.

[18] Hendricks, E. S., Falck, R. D., Gray, J. S., Aretskin-Hariton, E., Ingraham, D., Chapman, J. W., Schnulo, S. L., Chin, J., Jasa, J. P., and Bergeson, J. D., "Multidisciplinary Optimization of a Turboelectric Tiltwing Urban Air Mobility Aircraft," *AIAA Aviation 2019 Forum*, 2019, p. 3551.

[19] "Uber Elevate. Uber air vehicle requirements and missions," https://s3.amazonaws.com/uber-static/elevate/Summary+Mission+and+Requirements.pdf (Accessed: 2 December 2022), 2018.

[20] Ning, S. A., "A simple solution method for the blade element momentum equations with guaranteed convergence," *Wind Energy*, Vol. 17, No. 9, 2014, pp. 1327–1345.

[21] Ning, A., "Using Blade Element Momentum Methods with Gradient-Based Design Optimization," *Structural and Multidisciplinary Optimization*, Vol. 64, No. 2, 2021, pp. 994–1014. doi:10.1007/s00158-021-02883-6.

[22] Du, Z., and Selig, M., "A 3-D stall-delay model for horizontal axis wind turbine performance prediction," *1998 ASME Wind Energy Symposium*, 1998, p. 21.

[23] Eggers Jr, A., Chaney, K., and Digumarthi, R., "An assessment of approximate modeling of aerodynamic loads on the UAE rotor," *Wind Energy Symposium*, Vol. 75944, 2003, pp. 283–292.

[24] Viterna, L. A., and Janetzke, D. C., "Theoretical and experimental power from large horizontal-axis wind turbines," Tech. rep., National Aeronautics and Space Administration, Cleveland, OH (USA). Lewis Research Center, 1982.

[25] Glauert, H., "Airplane propellers," *Aerodynamic theory*, Springer, 1935, pp. 169–360.

[26] Buhl Jr, M. L., "New empirical relationship between thrust coefficient and induction factor for the turbulent windmill state," Tech. rep., National Renewable Energy Lab.(NREL), Golden, CO (United States), 2005.

[27] Glauert, H., *The analysis of experimental results in the windmill brake and vortex ring states of an airscrew*, HM Stationery Office, 1926.

[28] Clarke, M., and Alonso, J. J., "Lithium–Ion Battery Modeling for Aerospace Applications," *Journal of Aircraft*, Vol. 58, No. 6, 2021, pp. 1323–1335.

[29] Zou, Y., Hu, X., Ma, H., and Li, S. E., "Combined state of charge and state of health estimation over lithium-ion battery cell cycle lifespan for electric vehicles," *Journal of Power Sources*, Vol. 273, 2015, pp. 793–803.

[30] Gill, P., Murray, W., and Saunders, M., "SNOPT: An SQP Algorithm for Large-Scale Constrained Optimization," *SIAM Journal of Optimization*, Vol. 47, No. 1, 2005, pp. 99–131.

[31] Revels, J., Lubin, M., and Papamarkou, T., "Forward-Mode Automatic Differentiation in Julia," *arXiv:1607.07892 [cs.MS]*, 2016. URL https://arxiv.org/abs/1607.07892.